Weld Pool Impedance for Pool Geometry Measurement: Stationary and Nonstationary Pools

A. S. Tam

D. E. Hardt

Laboratory for Manufacturing and Productivity,
Massachusetts Institute of Technology,
Cambridge, MA 02139

The most elusive quantity in describing weld pool geometry is the depth, since it cannot be directly observed; yet it is the most important quantity to be regulated during welding. This paper addresses the problem of depth feedback measurement for full penetration welds, where the objective is to completely melt the cross section. It has been demonstrated that the existence and size of a full penetration weld can be detected by measuring the mechanical impedance of the resulting weld pool. Previous work in modeling this phenomenon has been limited to stationary welds, and experiments have either used impractical measurement methods or have not provided conclusive results. In this paper, a model of pool motion is developed that applies to both the stationary and moving weld case, and the pool motion is detected directly from changes in the arc voltage. A description of pool motion is derived from an elliptical membrane model, and the total system transfer function, including arc and pool dynamics is derived. A series of experiments demonstrates that the pool motion can indeed be detected for the moving pool case. However, the exact determination of pool oscillation frequencies requires knowledge of the pool perimeter geometry, since the elliptical system has many closely spaced eigenvalues arising from both symmetric and antisymmetric mode shapes.

Introduction

The study of welding process control has been dominated by research into methods of in-process sensing of the weld pool geometry. While it has been shown feasible to measure the top-side pool geometry using video methods [Sweet et al. (1983), Richardson et al. (1982)], the penetration or backside bead width have yet to be measured in a practical fashion, particulary if a top-side sensor location is required.

The concept of using weld pool motion as a pool geometry sensing method was proposed by Hardt et al. (1982) and later demonstrated by Zacksenhouse and Hardt (1983) and Richardson and Renwick (1983), and most recently by Sorensen (1985). The concept is based on the fluid dynamics of a pool constrained by a solid container and by significant surface tension forces (i.e., a small shallow pool, not a "pond" or "lake"). Such a pool will exhibit a surface motion that is a function of external forces, the properties of the fluid, the surface tension, and the *shape* of the container. Thus, if this motion can be excited, measured, and related to the pool geometry, a means of sensing pool shape will exist.

Further, for the Gas Tungsten Arc Welding Process (GTAW), since the pool can be forced using the arc plasma and the pool motion detected using the arc voltage, no additional instrumentation would be necessary to accomplish this sensing. Therefore, the promise of pool dynamics as a sensing method is to provide topside pool depth information simply by modulating the current and performing signal processing on the resulting arc voltage. All work to date has concentrated on GTAW and extension to other processes are not clear at this time.

All of the above work has suggested that the pool motion exists for both stationary and moving pools, however, neither models for the pool dynamics while moving, nor a complete analysis of arc-pool dynamics have been forwarded. This has in turn led to incomplete, ambiguous or impractical results. This work seeks to rectify these shortcomings by developing a model of the moving pool case that includes the arc-pool dynamics, and that examines closely the factors that corrupt the measurement of pool motion from arc voltage. All analysis and experiments are on full penetration welds, since the use of surface oscillations for detecting pool shape in partial penetration welds has been shown to be impractical, both analytically [Hardt, (1986)], and experimentally [Sorenson (1985)].

Pool Dynamics

Oscillations of a Stationary Pool. The goal of the following models is to obtain expressions for the dominant frequencies and modes of oscillation of a weld pool; they are not intended to predict the complex fluid flow within the molten region. For this reason, the internal effects of electromagnetic stirring, thermal gradients, etc. are not considered. The models only predict the gross motion of the

Contributed by the Dynamic Systems and Control Division for publication in the JOURNAL OF DYNAMIC SYSTEMS, MEASUREMENT, AND CONTROL. Manuscript received by the Dynamic Systems and Control Division November 16, 1987; revised manuscript received March 8, 1988 and September 19, 1988. Associate Editor: A. G. Ulsoy.

molten region based upon boundary conditions imposed by the geometric constraints.

The welds to be studied are full penetration welds on a thin steel plate. To obtain a simple model, the molten pool is assumed to be suspended by surface tension from the surrounding solid weldment. The stationary weld is modeled as having a circular surface of radius a, and the thickness of the molten region is also assumed to be small compared to its diameter. The pool can thus be modelled as a thin membrane that satisfies the wave equation:

$$\nabla^2 f = \frac{1}{c^2}\frac{\partial^2 f}{\partial t^2} \tag{1}$$

where f is the vertical deflection at point (x, y),
$c^2 = T/\rho$,
ρ is the surface density of the membrane (mass/area) and
T is the surface tension.

The classical solution of this equation using separation of variables leads to the expression:

$$f(r, \theta, t) = \sum_{n=0}^{\infty}\sum_{m=1}^{\infty} A_{mn} J_n\left(\frac{\omega_{mn} r}{c}\right)\cos(m\theta)\cos(\omega_{mn} t) \tag{2}$$

where $J_n(\xi)$ is a Bessel function of the first kind, and θ and ω_{mn} are the mode shapes and frequencies. To determine the mode frequencies, the boundary condition of zero displacement around the perimeter: $f(a, \theta, t) = 0$ is applied, which requires

$$J_n\left(\frac{\omega_{mn} a}{c}\right) = 0 \tag{3}$$

where a is the pool radius.

This equation thus determines the oscillation frequencies of the system ω_{mn}. For this analysis, only the first two modes will be considered, (J_0 and J_1).

The first and second modal frequencies are given by:

$$\frac{\omega_0 a}{c} = 2.405; \quad \frac{\omega_1 a}{c} = 3.832 \tag{4}$$

To obtain values of the first two modal frequencies, the following material properties and dimensions are inserted into the equation. The values are based on the weldment used in subsequent experiments—3.1 mm. (0.125 in.) thick mild steel pipe. The membrane modal assumes a surface density based on area instead of volume. For the weldment used, the surface density is found by the product of the density of steel and the thickness of the pipe.

$$\begin{aligned} T &= 1.0 \text{ N/m} \\ \rho &= 7.8 \times 10^{-6} \text{ kg/mm}^3 \\ h &= 3.1 \text{ mm.} \end{aligned} \tag{5}$$

The resulting first and second mode frequencies are given by:

$$\omega_0 = \frac{156}{w} \text{ Hz.}; \quad \omega_1 = \frac{249}{w} \text{ Hz.} \tag{6}$$

where w is the pool width in mm. For a typical large stationary pool with width of 6 mm, $\omega_0 = 26$ Hz. and $\omega_1 = 42$ Hz.

The mode shapes of the first two oscillation modes are that of a gross up and down motion of the pool and a sloshing mode where half of the pool is 180 deg out of phase with the other half (see Fig. 1). For free oscillations, the coefficients A_{mn} of equation (2) decrease with n, so the amplitude of the first mode should be dominant.

Extension to a Moving Pool. A similar analysis can be made for a moving pool. To observe the effect of the altered pool shape on its natural frequencies, the pool is modelled as having an elliptical shape. Again, the membrane vibration

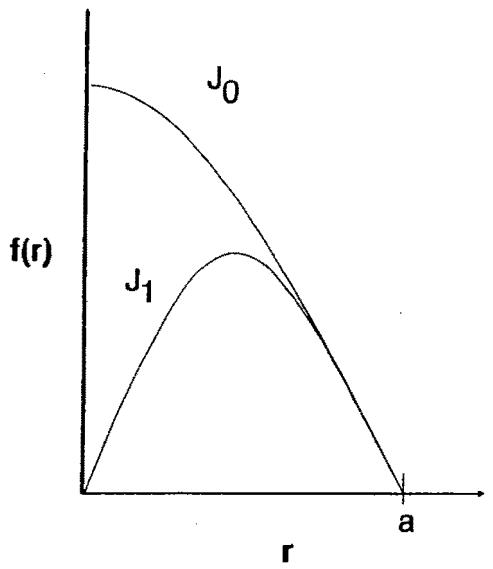

Fig. 1 First two mode shapes for a circular membrane. The first mode, J_0, is symmetric about the pool center. The second mode, J_1, is a sloshing mode and is antisymmetric about a diameter.

must satisfy the wave equation [McLachan (1951)]. Let the elliptical coordinates be described by the variables ξ and η. These are analogous to the polar coordinates r and θ, and ξ = constant now describes points on an ellipse; η has the same role as θ. With the change of coordinates

$$\begin{aligned} x &= \kappa \cosh(\alpha)\cos(\eta) \\ y &= \kappa \sinh(\xi)\cos(\eta) \end{aligned} \tag{7}$$

the wave equation becomes

$$\frac{1}{c^2}\frac{\partial^2 f}{\partial t^2} = \frac{1}{\alpha^2\cosh^2(\xi) - \alpha^2\cos^2(\eta)}\left(\frac{\partial^2 f}{\partial \xi^2} + \frac{\partial^2 f}{\partial \eta^2}\right) \tag{8}$$

This equation can once again be solved by separation of variables by assuming a product solution of the form

$$f(\xi, \eta, t) = \Xi(\xi) H(\eta) T(t) \tag{9}$$

The separated equations are

$$\begin{aligned} \Xi'' + [\alpha^2\omega^2\cosh^2(\xi) + \lambda]\Xi &= 0 \\ H'' - [\alpha^2\omega^2\cos^2(\eta) + \lambda]H &= 0 \\ T'' + \omega^2 T &= 0 \end{aligned} \tag{10}$$

The first two of these are forms of Mathieu's equation. The general solution has the form

$$\begin{aligned} f(\Xi, u, t) = &\sum_{m=0}^{\infty} C_m Ce_m(\xi, q) ce_m(\eta, q)\cos(\omega_m t + \epsilon_m) \\ &+ \sum_{m=1}^{\infty} S_m Se_m(\xi, q) se_m(\eta, q)\cos(\omega_m t + \epsilon_m) \end{aligned} \tag{11}$$

The mode shapes are as follows:

$Ce_{2n}(\xi, q) ce_{2n}(\eta, q)$ is symmetric about both the major and minor axes.

$Ce_{2n+1}(\xi, q) ce_{2n+1}(\eta, q)$ is symmetric about the major axis and antisymmetric about the minor axis.

$Se_{2n}(\xi, q) se_{2n}(\eta, q)$ is antisymmetric about both the major and minor axes.

$Se_{2n+1}(\xi, q) se_{2n+1}(\eta, q)$ is antisymmetric about the major axis and symmetric about the minor axis.

Since an ideal plasma jet should coincide with the axis of travel, (the major axis of the ellipse), the $Se(\xi, g) se(\eta, q)$ modes should not be excited. However, the arc will be

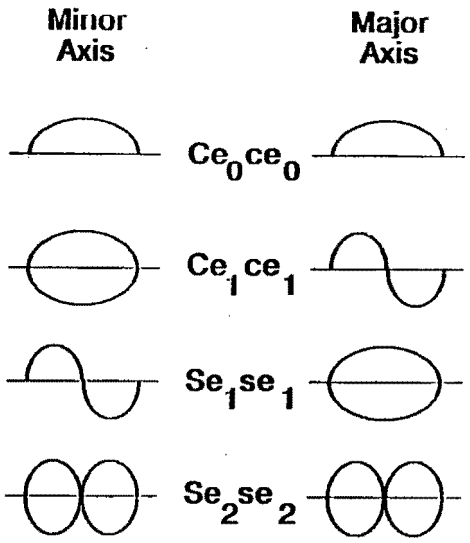

Fig. 2 Mode shapes for an elliptical membrane as viewed parallel to the minor and major axes

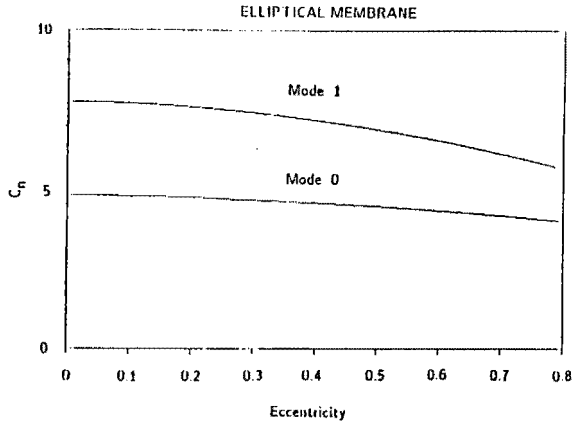

Fig. 3 Frequency coefficient C_n versus eccentricity ϵ. The modal frequency is given by $\omega_n = 203\ C_n/w$ where ω_n is in Hz and w is in mm.

centered over one end of the ellipse and the force distribution will be antisymmetric about the minor axis. All the $Ce(\xi, q)ce(\eta, q)$ modes will thus be expected in the pool motion.

Again, considering just two modes, the first mode, Ce_0, is analogous to the first mode of the circular membrane with the whole surface undergoing vertical displacement in the same direction. The second mode, Ce_1, corresponds to a sloshing mode where half of the surface is raising while the other half is falling (Fig. 2). The boundary conditions require

$$Ce_n(\xi_0, q_n) = 0$$

$$\xi_0 = \cosh^{-1}(1/\epsilon) \tag{12}$$

where ϵ is the pool eccentricity and is given by

$$\epsilon = [1 - (a^2/b^2)]^{1/2} \tag{13}$$

where a is the minor radius of the ellipse and b is the major radius of the ellipse.

The natural frequencies arising from these equations are

$$\omega_n = k_n(T/m)^{1/2} \tag{14}$$

where the nth modal coefficient k_n is given by

$$k_n = \frac{2q_n}{a\epsilon} \tag{15}$$

This equation must be solved numerically to yield values for q_n. The equations for these modes were approximated using a series expansion and values of q_0 and q_1 were found for different eccentricities. These values may be approximated as follows:

$$\begin{aligned} q_0 &= 2.03 \times 10^{-2} e^{(5.98\,\epsilon)} \qquad 0.17 < \epsilon < 0.94 \\ q_1 &= 4.346\ \epsilon^{2.064} \qquad\qquad 0.05 < \epsilon < 0.77 \end{aligned} \tag{16}$$

Using the values from equation (5) in equation (15) now gives natural frequencies of

$$\omega_n = 203\frac{C_n}{w}\ \text{Hz}. \tag{17}$$

where C_n is dependent on eccentricity and is plotted in Fig. 3.

For zero eccentricity, corresponding to a circular pool, the values of the natural frequencies reduce to those predicted by equation (6). As eccentricity increases, the mass of the oscillating fluid increases, but the perimeter also increases, leading to a higher system stiffness owing to increased surface tension effects. The resulting effect of the eccentricity on the first frequency is small, with a slight decrease as eccentricity increases. The second mode shows a greater sensitivity to eccentricity. Intuitively, this result is valid since the sloshing effect would be more dependent on the mass of the fluid and less on the boundary surface tension effects. The increase in pool mass would thus have a greater effect than the increase in pool perimeter.

Model Limitations. To obtain a simple model the pool was assumed to be a thin membrane with essentially perpendicular liquid/solid interface. In the real welding situation, this interface itself is not clearly defined and would more likely follow a taper from the top surface to the back surface. The effect of the added dimension was evaluated [Tam (1986)] by studying a pool with a circular section but with linearly tapering walls. In effect, the tapering wall boundary condition dictates a natural frequency that varies as one progresses vertically into the pool, bounded by the boundary conditions on the top surface and those on the bottom surface. However, for this case, the conflicting boundary conditions indicate that the membrane model is no longer valid and a continuum model must be used to accurately predict the actual frequencies.

The elliptical model of the moving pool is also a simplification of its actual pear, or tear drop shape of the molten pool. The "eccentricity" and "pool width" now must be considered to vary as one progresses from the front of the pool to the rear. Once again, whereas a unique frequency is predicted for the modes, a continuous range of frequencies may be expected, arising from the differing boundary conditions on the surface. Also, the effect of impurities has been ignored in this analysis, and it is well documented that presence of trace elements can greatly affect the temperature dependence of surface tension in the molten region and will thus affect the modal frequencies [Sundell et al. (1986)].

In summary, the model presented predicts the first two modal frequencies of the weld pool. For a stationary pool, the frequencies are related to the pool diameter, whereas, for a moving pool, the elliptical model provides a further relationship between the frequencies and the eccentricity of the pool. The frequency of the first two modes, along with the *ratio* of these frequencies, will provide information about the pool width and the pool eccentricity. Information about nonvertical pool walls and varying pool eccentricity may be inferred from the range of frequencies about the peaks. The first mode should provide more information about the nature of the wall since this mode is less sensitive to eccentricity and is likely to be more sensitive to the wall taper. Likewise, the second or sloshing mode would provide more information about the pool eccentricity.

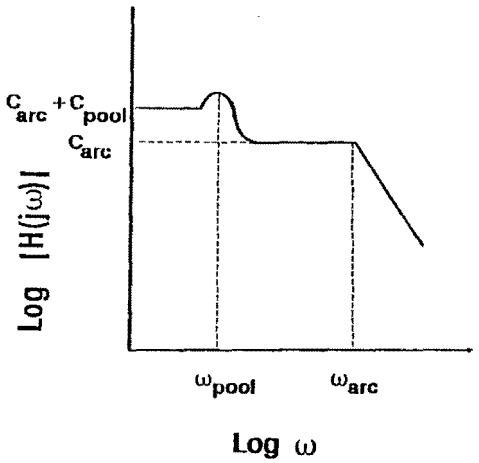

Fig. 4 Theoretical frequency response of measured arc voltage to arc current. Arc dynamics introduce a second order zero; if the voltage drop across the pool is small compared to that across the arc, the transfer function may appear nearly flat out to the bandwidth of the arc.

Arc-Pool Dynamics

Excitation of the Weld Pool. The response of the weld pool can be measured by applying a force to the pool and detecting the resulting pool displacement. As has been established by Converti (1981), the plasma jet momentum from the welding arc, resulting from the expansion of the current path from the electrode to the weldment, can be used to provide this force. The change in momentum (force) on the molten pool surface is given by

$$F=(\mu/8\pi)\,I^2[1+2\ln(R_2/R_1)] \tag{1}$$

where μ is the magnetic permeability for free space
I is the weld current
R_1 is the arc radius at the tip
R_2 is the arc radius after expansion.

This equation illustrates the quadratic relationship between current and force. If sufficient excitation can be obtained with small modulation amplitudes, the relationship may be linearized about the average current; however, if large excursions are needed, the nonlinearity must be taken into account.

The next step in the signal analysis is the measurement of the motion of the molten pool surface. The arc length, which is directly coupled with arc voltage, can be used as a transducer between the mechanical motion of the pool and electrical changes. The arc voltage can be broken up into several components including the anode and cathode drops, the drop across the arc column. While the voltage drops across the cathode and the anode can be assumed constant, the drop across the arc plasma is a function of the distance between the torch tip and the molten pool surface.

Previous approximations of the effect of pool motion on arc voltage have taken a rather simple approach [Sorenson (1985), Zackenhouse (1982)], and have in effect measured the voltage change caused by the net elevation change of the torch, i.e., as if the pool contour did not change shape. This approach yields typical voltage changes in the range of 0.8 V/mm, which should in turn give a strong signal for pool motion analysis. In practice this is not the case, however, and can be explained by the fact that the voltage changes observed are not only those caused by the displacement of the pool center, but an average change across the pool surface. For example, if the surface is assumed to be a half sine in contour, the actual voltage change integrated over the pool surface is only 46 percent of that obtained for bulk motion of the pool.

Expected Transfer Function/Power Spectrum. If the excursions of the signals about a mean operating point are small, the system can be linearized and a transfer function found between the input current and the measured voltage. This transfer function reflects the change in arc voltage caused by pool motion *and* the voltage change caused by current changes in the arc column. To include the arc columns response in the transfer function, one begins with the basic VI relationship for the system:

$$\Delta V=IR_{arc}+IR_{pool} \tag{19}$$

where IR_{pool} is the drop associated with arc column length changes caused by pool motion.

Under stable arc conditions, the voltage drops across the anode and the cathode have been found to be constants and have been ignored in the dynamic analysis, however, the plasma arc has its own electrodynamics and cannot be ignored. Converti (1981) has found that the argon arc has a bandwidth of approximately 1 kHz. Since the voltage drop across the arc accounts for a large component of the measured voltage, it must be included in the model. The system transfer function can thus be modeled as a sum of the transfer function of the arc and the pool:

$$H(s)=\frac{V}{I}(s)=H_{arc}(s)+H_{pool}(s) \tag{20}$$

If both systems are modeled as second order transfer functions, the total transfer function has the form:

$$H(s)=\frac{As^2+Bs+C}{(s^2+2\zeta_{arc}\omega_{arc}s+\omega_{arc}{}^2)(s^2+2\zeta_{pool}\omega_{pool}s+\omega_{pool}{}^2)} \tag{21}$$

where $A=C_{arc}\omega_{arc}^1C_{pool}\omega_{pool}^2$
$B=2\omega_{arc}\omega_{pool}(\zeta_{arc}\omega_{pool}+\zeta_{pool}\omega_{arc})$
$C=\omega_{arc}^2\omega_{pool}^2(C_{arc}+C_{pool})$

The effect of including the arc electrodynamics is to introduce two zeros into the transfer function. The natural frequency of the weld pool was predicted to be below 100 Hz whereas that of the arc is 1kHz. The expected frequency response is shown in Fig. 4, where the first dip corresponds to the natural frequency of the pool and the second dip corresponds to the natural frequency of the arc. From a frequency of zero up to the natural frequency of the pool, the response will have a magnitude of $C_{arc}+C_{pool}$. The response will then drop, but level off again at a magnitude of C_{arc}. It will remain at this level out to the bandwidth of the pool, when it will roll off at a rate of 40 dB/decade.

The magnitude of the dropoff at the pool's natural frequency thus depends on $C_{pool}/(C_{arc}+C_{pool})$. Also, these constants may be assumed to be proportional to the voltage drops across the corresponding section. For argon, the total voltage drop across the arc in on the order of 10 volts whereas that caused by pool motion is less than 1 volt. The dropoff at the pool's natural frequency is thus quite small and may be easily obscured.

This modified transfer function agrees with the experimental results observed by Zacksenhouse (1981) and the small magnitude of the pool contribution in argon coupled with the noisy spectrum explain the inability to detect a dropoff at the pool's natural frequency. The direct measurement of the back bead motion used by Zacksenhouse and Hardt (1983) eliminates $H_{arc}(s)$, thus the transfer function obtained there was simple second order.

Experiments

To examine the actual response of the arc-pool system, a series of experiments were performed using autogenous Gas Tungsten Arcs. A schematic of the apparatus is shown in Fig. 5. The weldment used throughout the experiments was 171 mm (6.75 in.) diameter, 3.1 mm (0.125 in.) thick mild steel

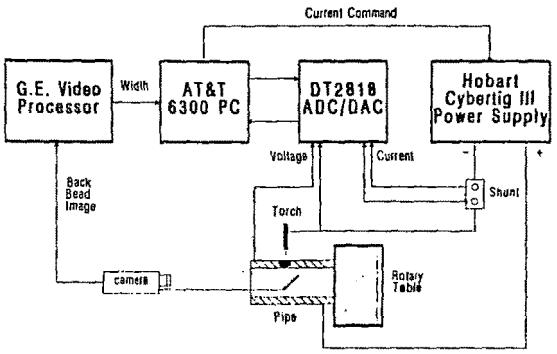

Fig. 5 Schematic representation of experimental setup

pipe. The section to be welded was clamped in a three jaw chuck mounted on a vertical rotary table. A Heliarc HG-20 water cooled torch was mounted on a stand which could be moved to position the electrode, a 2.4 mm (0.094 in.) diameter 2 percent thoriated tungsten electrode with a 60 deg included tip angle. The power supply was a Hobart CyberTig III GTA welding supply rated up to 150 A continuous current with a peak capacity of 200 A. The unit is a state-of-the-art inverter design current controller capable of the high bandwidth (−3dB @ 2 kHz) required in the modulation used in exciting the weld pool. The gas shielding used was either high purity Argon fed at 50 cfh or high purity Helimum fed at 160 cfh.

To obtain a measurement of the back-bead width, a General Electric Optomation Instrument Vision System was used to view the back-bead directly. The back-bead width was measured on the scan line passing through the centroid of the molten region and then sent out through a parallel port to the host computer.

The arc voltage was measured across the "cold" end of the welding electrode and a point on the weldment (analog ground). The arc current was measured by sensing the voltage drop across a shunt placed in series between the power supply and the torch. Sampling rates during experiments were all above 500 Hz, and all signals were passed through 150 Hz fourth order low pass Butterworth filters.

Several different waveforms for modulating the current and therefore the force were considered including pure sines, pulses, white noise, and pulse modulated white noise. The first two allow simple time domain identification, but tend to modify the welding process directly and also lead to slow identification, while pure white noise leads to a lack of separation between electrically and mechanically induced changes in the arc voltage.

Pulse modulated white noise was developed in an attempt to separate the dynamics of the molten pool from those of arc. It is created by amplitude modulation of an offset square wave by band limited white noise. Each pair of positive-negative pulses has the same random amplitude determined by a white sequence. The modulation and its frequency spectrum is shown in Fig. 6. The advantage of this modulation is that the pulse frequency can be chosen to be greater than the bandwidth of the pool but less than of the arc. The pool will then only see a white noise input while the modulation would be providing much more energy input than the equivalent white noise. Meanwhile, the voltage changes caused by the nonlinear arc resistance will tend to cancel out.

Both the white noise and pulse modulated white noise signals were generated in software by the computer. The random sequences were found to satisfy Chi-squared tests and were good approximations to a white sequence. The output sample frequency determined the maximum bandwidth of the sequence.

Power Spectrum Estimation. If the arc-pool system were

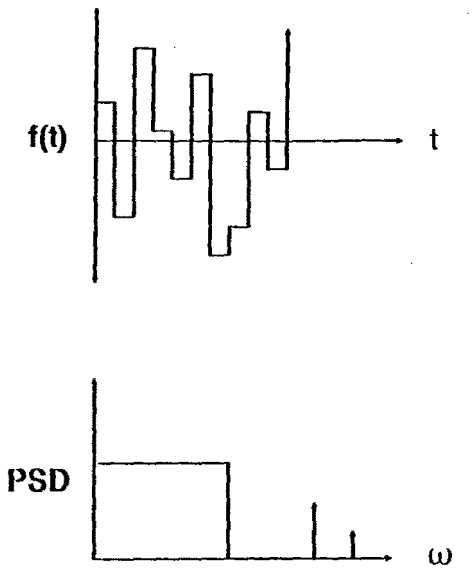

Fig. 6 (a) Pulse modulated white noise input. (b) Theoretical power spectrum contains power of band limited white noise as well as power of pulses.

indeed linear, or if small curent modulation levels could be used, the system transfer function could be found (as done by Zacksenhouse and Hardt (1983)) from:

$$H(j\omega) = \frac{\Phi_{fg}(j\omega)}{\Phi_{ff}(j\omega)} \tag{22}$$

where $H(j\omega)$ is the transfer function between the system input, $f(t)$ and the output $g(t)$,
$\Phi_{fg}(j\omega)$ is the DFT of the cross-correlation $\phi_{fg}(t)$,
and $\Phi_{ff}(j\omega)$ is the DFT of the auto-correlation $\phi_{ff}(t)$.

This calculation has the advantage that it is insensitive to noise in the input or in the measurement as long as the each noise is uncorrelated with the input. Therefore, if the input and output of a linear system can be sampled, their values may be processed to obtain a discrete system transfer function.

Unfortunately, the voltage-current relationship is nonlinear as is the current-plasma force relationship. The relationship between the system input, arc current, and the system output, arc voltage, is only linear, therefore, for very small current excursions. The current modulations necessary to excite the weld pool may not fall into this region and equation (22) may be invalid.

Accordingly, for all the experiments described here, the system is described by the ratio of the power spectral density of the output voltage to the input current. This allows for both high levels of current modulation and for nonideal frequency content in the input waveform.

The power spectral density (PSD) of a signal can be estimated by taking the DFT of the autocorrelation of the signal [Tretter (1976)]. This resulting individual PSD has an extremely high variance and is by itself a poor estimate of the actual power in the signal. One way to obtain a better estimate is to average a series of estimates. The data can be blocked off into separate sections, each of which provides a separate estimate. Certain "data windows" may be used to obtain a smooth estimate and eliminate leakage effects [Brigham (1974)]. The average of these estimates then provides a good representation of the actual PSD.

The problem with this method of analysis is the difficulty of providing an accurate magnitude for the power at a given frequency. However, this analysis for pool shape is interested not so much in the magnitude of the peaks as in their existence and the frequencies at which they occur, thus such estimates obtained are adequate for our purposes.

The sampled signals were broken up into blocks, each of

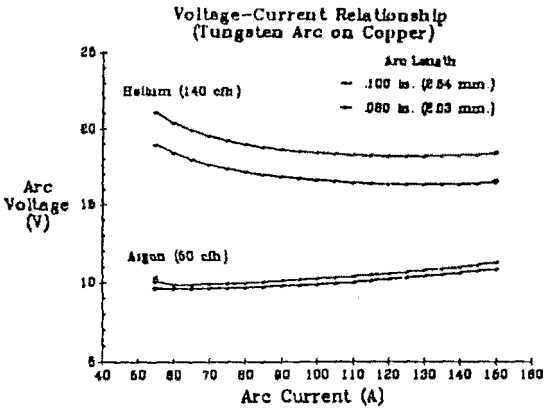

Fig. 7 Voltage-current relationship for a tungsten arc on a water cooled copper plate

which was then windowed and the PSD calculated by taking the FFT of the autocorrelation. A running average was kept of all the PSDs to provide the final estimate. The ratio of the PSDs was then obtained by the dividing the value of the voltage PSD by that of the current PSD at each discrete frequency. Standard values used were: a FFT length of 1024, window length of 256, with 2048 data points sampled at 1024 Hz. The Hanning window was determined to yield the smoothest PSD estimate and was used for most of the analysis. The signals were also high pass filtered prior to the estimate to ensure numerical stability in the summations necessary for averaging the PSDs.

A typical experiment would be conducted as follows. The arc was struck, and after a set delay, the current was modulated and the voltage and current signals sampled. A representative section of the digitized signals could be viewed. The initial and final widths obtained from the vision system were used to predict the frequencies of the first two modes based on equation (17).

Results

Arc Voltage-Current Relationship. It has been assumed that the arc is essentially a simple gain over the frequency range of expected pool oscillations. To precisely determine the nature of this response for our particular system, the dynamics of the arc were measured independent of pool motion by using a water cooled copper block as the weldment. A fixed arc length was then set using gauge blocks. The current was varied between 50 A and 150 A and the corresponding arc voltage measured. This test was performed for arc lengths of 2.54 mm (0.100 in.) and 2.032 mm (0.080 in.). Both helium and argon were used as shielding gases. The result is shown in Fig. 7.

As can be seen, the relationship is not linear and the nonlinearity is different for each gas. The helium arc has a decreasing slope up to approximately 100 A, after which the curve becomes nearly independent of current. The argon arc has a positive slope for currents greater than 60 A. The conclusion is that variations in the measured voltage will have components caused by this nonlinear arc resistance.

The voltage-current relationship also provides an indication of the magnitude of the voltage change caused by pool motion. As shown earlier, the voltage change can be estimated by measuring the change caused by a change in arc length and scaling the number by a factor of 0.46. The expected voltage difference is 1.6 V/mm for a helium arc and 0.4 V/mm for an argon arc. As noted by Sorensen (1985), since the helium arc has roughly twice the arc voltage of an argon arc of the same length but provides four times the voltage sensitivity, pool motion should be easier to identify with helium shielding.

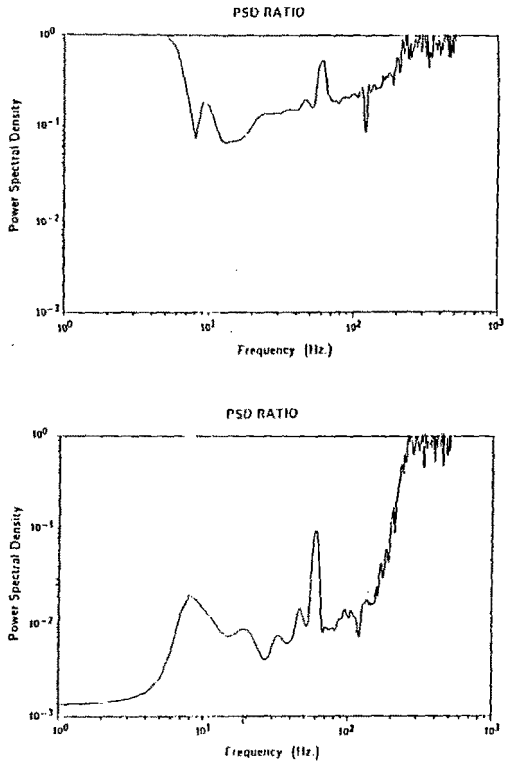

Fig. 8 PSD of Voltage/Current, copper block test. Output frequency = 300 Hz., average current = 100 A, and current amplitude = 10 A.
(*a*) argon shielding;
(*b*) helium shielding

The pulse modulated white noise (PMWN) was selected as the main excitation for further testing and its parameters were optimized for both argon and helium shielding. Tests were performed studying the effect of current amplitude and average value changes, as well as the average frequency.

These tests show that although helium shielding is preferable for its higher sensitivity to pool motion, the helium arc has detrimental voltage-current characteristics (compare Fig. 8 (*a*) and (*b*)) which would hinder detection of the natural frequencies of the pool. The argon arc provides a much smoother relationship but is less sensitive to pool motion, and the average current should be above 100 A with maximum amplitudes above 30 A and output frequency between 200 and 500 Hz.

Detection of Pool Motion for a Stationary Weld. Initially a white noise input test was performed to determine the arc-pool PSD. This was chosen to be consistent with the excitation employed by Zacksenhouse (1982) in her arc voltage output test. However, extremely erratic results were again encountered, and often no discernable response was obtained. The variance in the calculation of the power at each discrete frequency caused a certain amount of noise in the resultant PSD plot and this noise level may be sufficient to drown out the expected step.

As an alternative, pulse inputs similar to those used by Renwick and Richardson (1983), and Sorensen (1985) were employed. A steady state pool was developed with a constant current and with with argon shielding. A positive pulse was then applied and sampling started after the trailing edge of the pulse. Thus, during the sampling time, the system "sees" no excitation and the frequency peaks present in the voltage PSD should be caused solely by pool motion. Various average currents, current amplitudes, and arc lengths were used to obtain different pool sizes.

A typical voltage PSD is shown in Fig. 9. The plot displays many peaks, several of which are near the frequencies

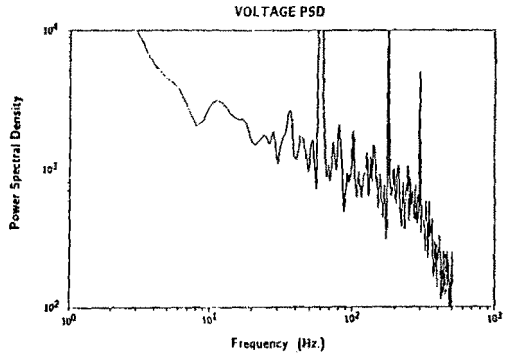

Fig. 9 Typical PSD of measured voltage for free oscillations after a pulse input with argon shielding

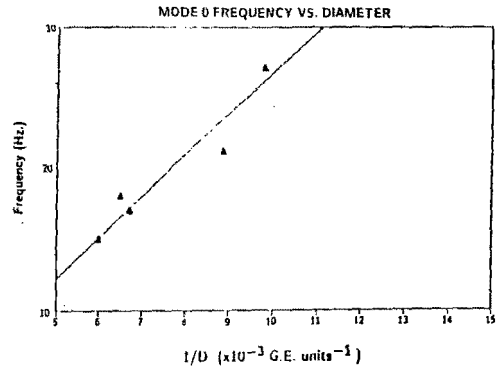

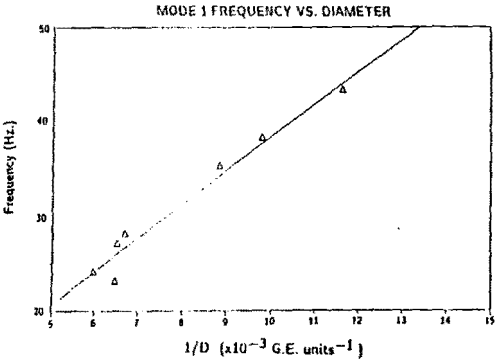

Fig. 10 Experimentally determined modal frequency versus measured pool diameter for a stationary, full penetration pool.
(a) first mode;
(b) second mode

predicted by the model. Peaks were chosen based on the model prediction of the first two frequencies and these frequencies plotted versus the inverse of the pool size. Figure 10(*a*) shows the relationship of the first modal frequency to pool size. A linear regression gives

$$f_0 = -2.1 + \frac{176}{w} \text{ Hz} \tag{23}$$

where f_0 is the first modal frequency and
w is the measured back pool width in mm.

Figure 10(*b*) shows the relationship of the second modal frequency to pool size. A linear regression gives

$$f_1 = 3.1 + \frac{213}{w} \text{ Hz} \tag{24}$$

where f_1 is the frequency of the second mode.

These relationships agree fairly well with the relationships predicted by the circular membrane model (equation (6)), and the negative offset in equation (23) accounts for the somewhat

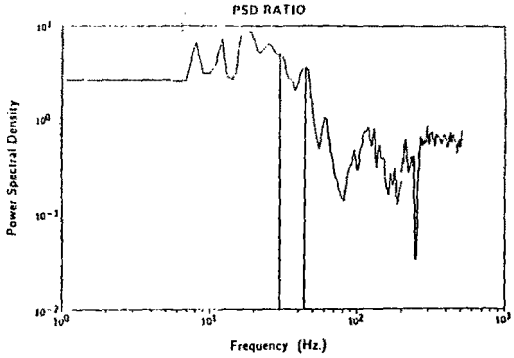

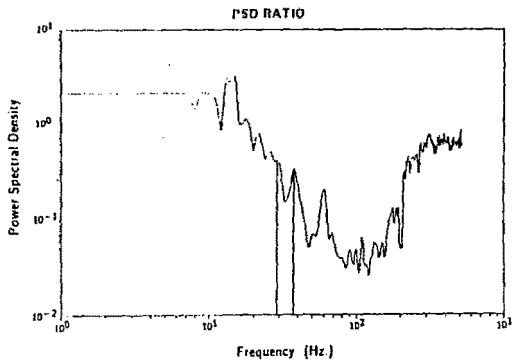

Fig. 11 PSD plots of voltage/current with PWMN and helium. (*a*) Output frequency = 500 Hz, average current = 80 A, current amplitude = 20 A, torch velocity = 134 mm/min. (*b*) Output frequency = 400 Hz, average current = 100 A, current amplitude = 30 A, torch velocity = 195 mm/min.

high value of 176 whereas the positive offset in equation (24) accounts for the low value of 213.

Though this experiment shows that the model can be used to predict a natural frequency given a pool size, the converse prediction is the one required in the measurement scheme necessary for a closed loop controller. The size and other geometric parameters of a pool must be deduced from the frequency plot. Figure 9 shows that the peaks caused by the pool are hidden among many other peaks, causing such a prediction based on the PSD alone to be almost impossible without other data. Moreover, such an excitation scheme is undesirable in a control sense since it is based on adding a pulse disturbance to an equilibrium state. The excitation also impies a nonsteady average heat input and may not be harmonious with a control strategy.

Detection of Oscillations of a Moving Pool. To develop a moving pool, the pipe was rotated by a servo motor to provide relative motion between the torch and the weldment. The relative velocity provided another parameter used to obtain weld pools of different sizes and eccentricities. The control program was able to read in a back bead width from the vision system and predict the first two frequencies based on the pool eccentricity.

Pulse modulated white noise (PMWN) was used as the current modulation, with helium as the shielding gas. Peaks were present in the ratio plot corresponding roughly to the predicted resonance vlaues, but these peaks were again hidden in a forest of peaks. Typical PSD plots of the signals and their ratios are shown in Fig. 11. Since these tests were done with helium shielding, each ratio plot shows a roll-off in frequency above 20 Hz. For some cases, this roll-off obscured a predicted peak in the range. However, when these peaks were detectable, they occurred at points slightly below those corresponding to a circular pool, thus confirming the eccentricity concept.

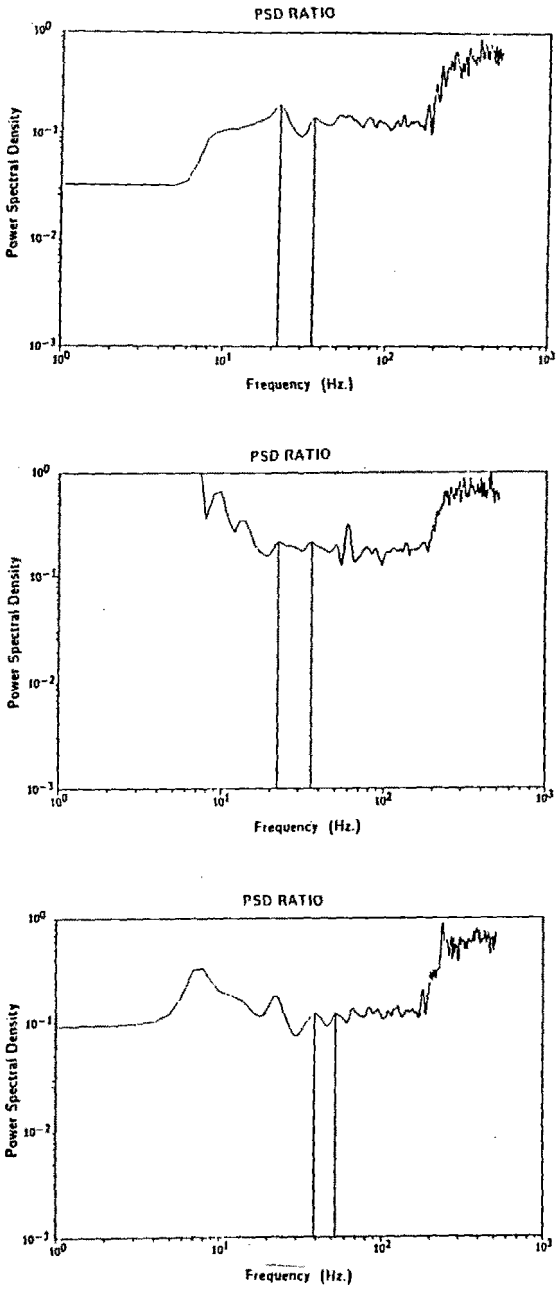

Fig. 12 PSD plots of voltage/current with PWMN and helium. Output frequency = 300 Hz, average current = 120 A, current amplitude = 30 A. (a) torch velocity = 93 mm/min. (b) torch velocity = 100 mm/min. (c) torch velocity = 127 mm/min.

Though helium provides a better signal to noise ratio for peak detection, the copper block experiments show that argon provides a much flatter spectrum ratio. Tests were thus made with argon shielding and the optimized PMWN parameters of 120 A average current, 30 A amplitude and 300 Hz output frequency. The welding speed was varied from 94 mm/min to 127 mm/min (3.7 to 5 in/min) to obtain pools of different widths and eccentricities.

Figures 12 (*a*), (*b*), and (*c*) show the results of these tests. As expected, the PSD ratio was flatter, and in most cases, the first two peaks above 10 Hz correspond closely to those predicted by the model. Since an eccentricity measurement was not available, the predicted frequencies could only be expressed as a function of the eccentricity. The frequency peaks all occurred below the values predicted for zero eccentricity, agreeing with the negative coefficients in the equations. Also, whereas some tests displayed fairly clear peaks at the predicted frequencies (Fig. 12 (*a*) and (*b*)), some displayed many peaks (Fig. 12 (*c*)).

In all the moving weld cases, the peak corresponding to the second or "sloshing" mode was almost as strong as that corresponding to the first mode. Since the torch tip is not positioned exactly above the minor axis, the arc momentum would be off center and would strongly excite this sloshing mode. Considering the origin of arc voltage changes at the pool surface, this mode would tend to average to zero because of its antisymmetry. However, in this case, the position of the torch tip off the minor axis would tend to make the contributions in leading half dominate, lessening the contributions of the trailing edge.

The PSD ratio plots of almost all the moving weld cases displayed many peaks besides those predicted by the first two modes. Some of these peaks may originate with higher order modes, or with the modes anti-symmetric with respect to the axis of torch motion. In the ideal case where the torch momentum is centered on the major axis, these modes should not be strongly excited. However, the centroid of the actual pool may not lie on the major axis, so that these modes are present.

Conclusions

Two models relating pool geometry parameters to frequency characteristics of pool motion have been presented. The intent is for the models to act as estimators or observers (in a closed loop system) that infer geometry information from the available measurements. The moving pool model provides a relationship between the first two modal frequencies and pool width as well as pool eccentricity. Deviations from these predictions may be used to identify the effects of a tapered solid/liquid interface, varying pool eccentricity, or surface tension changes caused by impurities.

Experiments have validated the presence of the predicted peaks in the frequency spectrum, but these peaks are often obscured in the noisy process. Contrary to other results [Sorenson (1985)], argon appears to be superior to helium since it provides a much flatter frequency relationship between arc voltage and arc current, although it does produce a lower output signal.

For a moving pool with an argon arc, the first two predicted peaks were often clearly identifiable. However, besides the first two predicted peaks, higher order modes were also often present in the power spectrum. The proximity of all these peaks makes a unique identification unreliable without other correlating data. The variance/resolution trade-off inherent in tis measurement scheme makes it only good for a rough measurement. Also, the time required to calculate the geometry parameters may cause too great a delay in the control scheme if this measurement were the only one available. With these exceptions in mind, weld pool impedance can be employed to augment other geometry measurements such as top-side vision and/or infrared measurements. This approach could provide valuable geometry information not otherwise obtainable for full penetration welds.

It is also well to notice that the presence of the higher order as well as the antisymmetric modes was not expected in such a strong showing. These modes could provide additional data for calculation of pool geometry, and their frequency values could be predicted by further numerical analysis of the Mathieu functions, thereby aiding in uniquely determining the alignment of the frequency peaks with the modes. Also, the arc dynamics played a strong hindering role in the analysis. Zacksenhouse (1982) attempted to eliminate this effect by estimating an arc resistance and subtracting a predicted voltage drop caused by this resistance from the voltage signal. However, the arc resistance is by no means linear and is at times a strong function of the

modulated white noise was an attempt to circumvent the arc dynamics and was somewhat successful. What is needed to obtain a good pool motion reading is to construct an observer that would predict the voltage contribution caused by arc dynamics and subtract this from the measured voltage. Like the pool oscillation predictions, this observer is non-linear and may require the need to measure nominal arc length as well as arc voltage and current.

Finally, what may be considered the greatest limitation with this measurement scheme is the fact that the voltage component from pool motion is actually an average drop across the whole pool. Further research is necessary in developing a measurement scheme which would either only reflect motions of the pool centroid, or better yet, motions at various points in the pool surface. The measurement of pool impedance through analysis of the arc voltage may always have the above problems associated with it. A better approach may be to somehow directly measure the motion of the pool surface using high speed video means.

References

1 Brigham, E. O., *The Fast Fourier Transform*, Prentice-Hall, Inc., NJ, 1974.

2 Converti, J., "Plasma Jets in Arc Welding," Ph.D. thesis, MIT Department of Mechanical Engineering, July 1981.

3 Hardt, D. E., Masubuchi, K. M., and Paynter, H. M., Unkel, W., Converti, J., and Zacksenhouse, M., "Improvement of Fusion Welding Through Modelling, Measurement and Real-Time Control," International Conference on Welding Technology for Energy Applications, Gatlinburg, TN, May 1982.

4 Hardt, D. E., "Measuring Weld Pool Geometry from Pool Dynamics," *Modeling and Control of Casting and Welding*, ASM, Jan. 1986.

5 McLachan, N. W., *Thoery and Application of Mathieu Functions*, Oxford, 1951.

6 Renwick, R. J., and Richardson, R. W., "Experimental Investigation of GTA Weld Pool Oscillations," *Welding Journal*, Vol. 62, 1983.

7 Richardson, R. W., Gutow, D. A., and Rao, S. H., "A Vision Based System for Arc Weld Pool Size Control," *Measurement and Control for Batch Manufacturing*, ASME Special Publication, 1982.

8 Sorensen, C. D., "Digital Signal Processing as a Diagnostic Tool for Gas Tungsten Arc Welding," Ph.D. thesis, MIT Department of Material Science, May 1985.

9 Sweet, L. M., Case, A. W., Corby, N. R., Kuchar, N. R., "Closed-Loop Joint Tracking, Puddle Centering and Weld Process Control Using an Integrated Weld Torch Vision System," *Control of Manufacturing Processes and Robotic Systems*, ASME Special Publication, 1983.

10 Sundell, R. E., Solomon, H. D., and Correa, S. M., "Minor Element Effects on Gas Tungsten Arc (GTA) Weld Penetration—Weld Pool Physics," *Advances in Welding Science and Technology*, ASM, 1966, pp. 53-58.

11 Tam, A. S., "Measurement of Weld Pool Geometry by Frequency Analysis of Pool Impedance," S. M. thesis, MIT Dept. of Mechanical Engineering, Oct. 1986.

12 Tretter, S. A., *Introduction to Discrete-Time Signal Processing*, Wiley, 1976.

13 Zacksenhouse, M., "Control of Penetration in Gas Tungsten Arc Welding: A Puddle Impedance Approach," SM thesis, MIT Department of Mechanical Engineering, May 1982.

14 Zacksenhouse, M., and Hardt, D. E., "Weld Pool Impedence Identification for Size Measurement and Control," *Transactions ASME, Journal of Dynamic Systems, Measurement and Control, 105*, No. 3, Sept. 1983.